NANO LETTERS

pubs.acs.org/NanoLett Letter

A Tale of Drug-Carrier Optimization: Controlling Stimuli Sensitivity via Nanoparticle Hydrophobicity through Drug Loading

Yen-Nan Lin, Sarosh Khan, Yue Song, Mei Dong, Yidan Shen, David K. Tran, Ching Pang, Fuwu Zhang,* and Karen L. Wooley*

Cite This: *Nano Lett.* 2020, 20, 6563−6571 Read Online

ACCESS | Metrics & More | Article Recommendations | Supporting Information

ABSTRACT: Interactions between drug molecules, nanocarrier components, and surrounding media influence the properties and therapeutic efficacies of nanomedicines. In this study, we investigate the role that reversible covalent loading of a hydrophobic drug exerts on intra-nanoparticle physical properties and explore the utility of this payload control strategy for tuning the access of active agents and, thereby, the stimuli sensitivity of smart nanomaterials. Glutathione sensitivity was controlled via altering the degree of hydrophobic payload loading of disulfide-linked camptothecin-conjugated sugar-based nanomaterials. Increases in degrees of camptothecin conjugation (f_{CPT}) decreased aqueous accessibility and reduced glutathione-triggered release. Although the lowest f_{CPT} gave the fastest camptothecin release, it resulted in the lowest camptothecin concentration. Remarkably, the highest f_{CPT} resulted in a 5.5-fold improved selectivity against cancer vs noncancerous cells. This work represents an advancement in drug carrier design by demonstrating the importance of controlling the amount of drug loading on the overall payload and its availability.

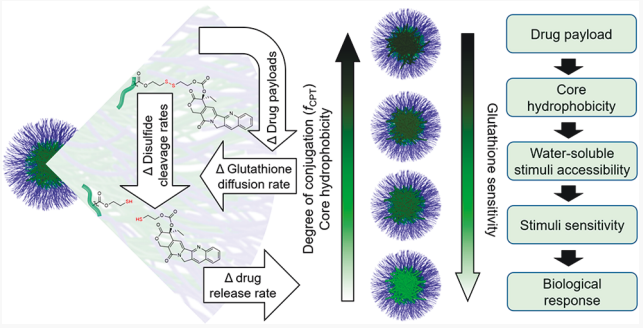

KEYWORDS: *Stimuli sensitivity control, glutathione-responsiveness, nanomedicine, core hydrophobicity, drug loading effect*

Over the past two decades of development of the field of nanomedicine, large bodies of work have sought to improve the performance of therapeutic agents by using nanoparticle carriers.[1−6] In general, emphasis has been on maximizing the drug payload to achieve transport and accumulation in a targeted tissue;[7−12] however, effects of the properties and extent of drug loading are often neglected. Drug loading may alter a nanocarrier's physiochemical properties in a loading-dependent manner, thereby influencing efficacy. For instance, loading of hydrophobic drug molecules within an amphiphilic nanoparticle framework may affect colloidal stability, size, shape, flexibility, internal accessibility, and other parameters,[12−16] each of which are important attributes affecting circulation time, clearance, biodistribution, and drug release.[17−21] Covalent drug conjugates enable sustained delivery without burst release during circulation, displaying minimized systemic toxicity and increased accumulations in targeted tissue.[3,9,16] Furthermore, stimuli-responsive properties provide a preferable spatiotemporal control over payload release, thereby improving therapeutic efficacy while reducing systemic toxicity.[2,5,7,8,22,23] Therefore, a thorough knowledge of the role that therapeutics play on the properties of nanomedicines as a function of payload level is of great importance, and control over drug-carrier-media interactions may provide an additional opportunity to tune physicochemical characteristics and biological performance of nanoformulations. As a proof of concept in this study, hydrophobic drugs were conjugated via stimulus-sensitive linkers along the hydrophobic backbone of amphiphilic block copolymers and assembled into nanoscopic micelles to investigate the importance of payload level on stimulus accessibility, drug release, and therapeutic efficacy and selectivity *in vitro*.

Glutathione (GSH) is an endogenous stimulus for redox-responsive drug carriers, because $[GSH]_{intracellular}$ (2−10 mM) > $[GSH]_{extracellular}$ (2−20 μM), and $[GSH]_{tumor\text{-}tissue}$ > $[GSH]_{healthy\text{-}tissue}$.[24−29] Since different drugs require different optimal release profiles,[4,30] controlling the sensitivity of GSH-triggered payload release is essential for optimizing redox-responsive carriers.[31] Different strategies have been reported to control the sensitivity of disulfide bonds,[32−36] which undergo reductive cleavage in a high-GSH environment and are commonly incorporated into nanomaterials to bestow redox-responsive properties.[1,37−42] However, these modulating

Received: June 3, 2020
Revised: July 31, 2020
Published: August 10, 2020

https://dx.doi.org/10.1021/acs.nanolett.0c02319
Nano Lett. 2020, 20, 6563−6571

Scheme 1. Synthetic Scheme for the Preparation of CPT-Conjugated PEG-*b*-PGC

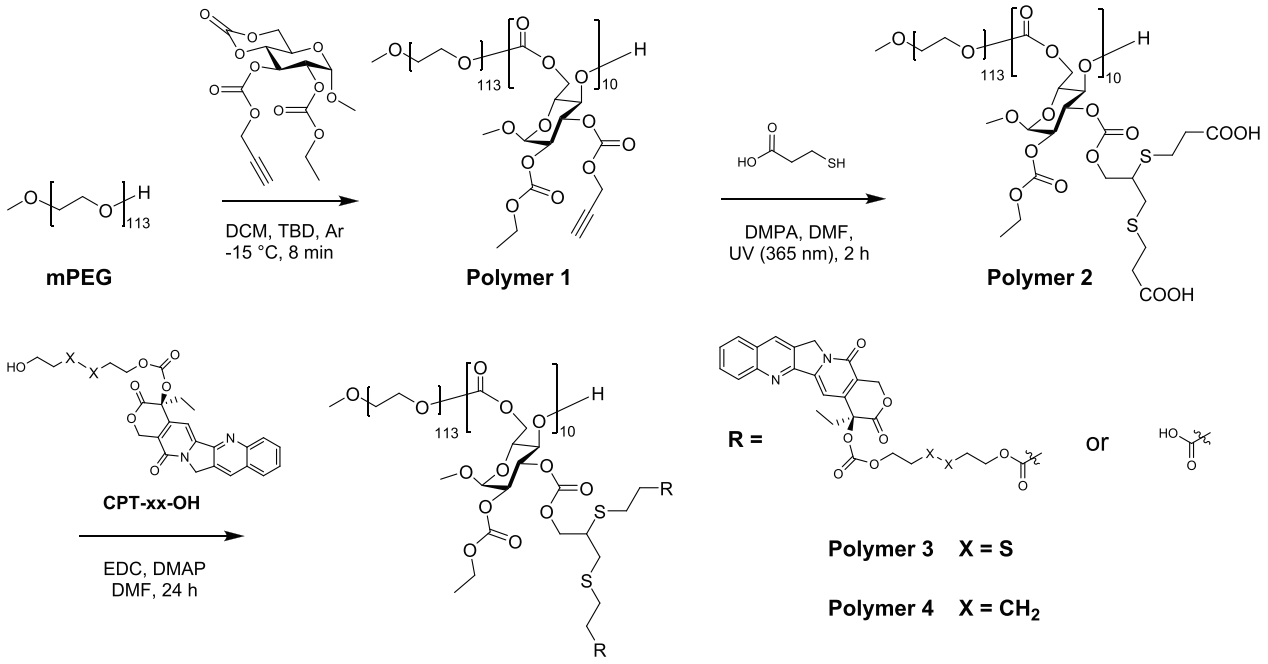

strategies often require specific chemical structures to achieve discrete GSH sensitivity, thereby elevating barriers for optimizing GSH-responsive drug carriers. For instance, thiol−disulfide exchange kinetics have been modulated by introducing steric or charged groups adjacent to the disulfide bond via precise sequence-controlled solid-phase peptide synthesis.[43,44] The GSH responsiveness of polymeric nanomaterials can be modulated by the placement of disulfide bonds in the backbone,[45−48] side chains,[46,49] or cross-links,[50,51] as well as by incorporating multistimuli-responsive properties.[52] Alternatively, substituting disulfide-linkages for other redox-sensitive linkages with different reductive potentials, such as Se−Se bonds,[53,54] can vary GSH sensitivity, yet this strategy is limited by the number of unique redox-labile linkages and potential toxicity of the elements involved.[55−57] Expanding facile approaches to control the sensitivity of nanomaterials toward GSH could be of paramount significance for the development and optimization of redox-responsive drug carriers.

Herein, we describe an approach that uses the active drug molecule directly, for both therapeutic effect and for alteration of nanoparticle physicochemical characteristics that provides for tuning of GSH sensitivity, thereby avoiding the incorporation of extra non-bioactive components, and creating an atom economical design of nanomedicines. To demonstrate this approach, the hydrophobic cancer chemotherapeutic camptothecin (CPT) was used, which, upon release, binds to the DNA topoisomerase I cleavage complex, thereby inhibiting DNA religation and resulting in apoptosis.[10,58−61] The degree of payload loading was altered by covalent conjugation of CPT via disulfide-linkages onto the backbone of poly(ethylene glycol)-*b*-poly(glucose carbonate) (PEG-*b*-PGC) (Scheme 1). The PEG block provides for hydrophilicity, whereas the sugar-based poly(glucose carbonate) (PGC) was selected for its sustainability, biocompatibility, degradability, multifunctionality for coupling with CPT, and ability to self-assemble into versatile nanostructures.[62−65] We hypothesized that GSH sensitivity could be controlled via tuning the core hydrophobicity of the nanomaterials. It was anticipated that increased CPT loading would result in increased hydrophobicity, thereby decreasing aqueous accessibility and limiting the diffusion of water and water-soluble molecules, leading to reduced access of GSH to disulfide-linkages in the core of PEG-*b*-PGC-based nanocarriers and lowered GSH sensitivity. The degree of CPT conjugation (f_{CPT}) is defined relative to the two carboxylic acids available at each PGC repeat unit, with no, low, medium, and high extents of CPT conjugation being targeted as f_{CPT} = 0, 0.15, 0.50, and 0.85, giving 0, 3, 10, and 17 CPTs per PEG-*b*-PGC chain. Due to the relatively high hydrophobicity of the PGC and CPT-PGC block segments in comparison to that of PEG, we speculated that the sugar segments would be primarily localized in the micelle cores, whereas the PEG segments would dominate the exterior surface of the nanocarriers in an aqueous environment.[11]

The CPT-conjugated PEG-*b*-PGCs were prepared by esterification between hydroxyl-functionalized CPT prodrugs (**CPT-xx-OH**) and carboxylic acid-functionalized PEG-*b*-PGC diblock copolymer (**2**). Polymer **2** was constructed by ring-opening polymerization (ROP) of a cyclic glucose carbonate monomer, followed by postpolymerization modification with mercaptopropionic acid (Scheme 1). Briefly, the diblock copolymer **1**, PEG_{113}-*b*-PGC$(EPC)_{10}$, was synthesized by organocatalyzed ROP of the bicyclic glucose carbonate methyl-2-*O*-ethyloxycarbonyl-3-*O*-propargyloxycarbonyl-4,6-*O*-carbonyl-*α*-D-glucopyranoside (GC(EPC)) at −15 °C in dichloromethane (DCM) with methoxy poly(ethylene glycol) ($mPEG_{113}$) as the macroinitiator and 1,5,7-triazabicyclo[4.4.0]-dec-5-ene (TBD) as the organocatalyst (Figures S1−S3). The carboxylic acid-functionalized polymer **2**, PEG_{113}-*b*-PGC-$(COOH)_{20}$, was then prepared by postpolymerization modification of **1** via photoinitiated thiol−yne click reactions using an excess of mercaptopropionic acid (>50 equiv relative to the alkyne groups) with 2,2-dimethoxy-2-phenylacetophenone (DMPA) as the photoinitiator (Figures S4 and S5). The CPT-conjugated polymers **3** and **4**, PEG_{113}-*b*-[$PGC(COOH)_x$-*co*-$PGC(CPT)_{20-x}$], were generated by postpolymerization modification of block copolymer **2** via 1-ethyl-3-(3-(dimethylamino)propyl)carbodiimide (EDC) mediated cou-

https://dx.doi.org/10.1021/acs.nanolett.0c02319
Nano Lett. 2020, 20, 6563−6571

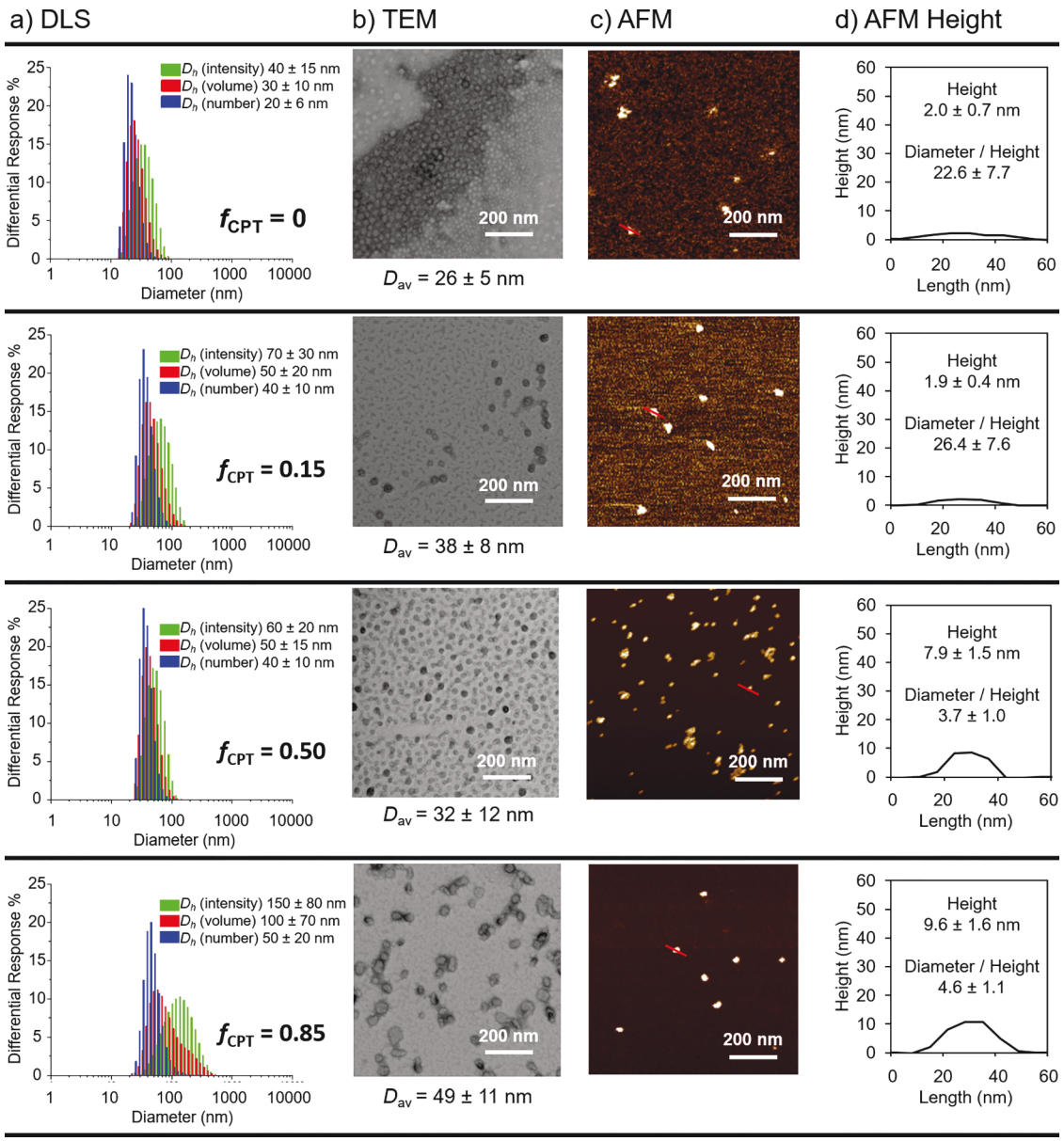

Figure 1. Morphological characterizations of the polymer assemblies using (a) DLS, (b) TEM, (c) AFM, and (d) AFM height profile. From top to bottom: polymer **2** (f_{CPT} = 0), polymer **3** (f_{CPT} = 0.15), polymer **3** (f_{CPT} = 0.50), and polymer **3** (f_{CPT} = 0.85).

pling reaction with (*S*)-4-ethyl-3,14-dioxo-3,4,12,14-tetrahydro-1*H*-pyrano[3′,4′:6,7]indolizino[1,2-*β*]quinolin-4-yl (2-((2-hydroxyethyl)disulfanyl)ethyl) carbonate (**CPT-ss-OH**) or (*S*)-4-ethyl-3,14-dioxo-3,4,12,14-tetrahydro-1*H*-pyrano-[3′,4′:6,7]indolizino[1,2-*β*]quinolin-4-yl (6-hydroxyhexyl) carbonate (**CPT-cc-OH**), respectively (Figures S6−S12). The f_{CPT} values were calculated from the ^{1}H nuclear magnetic resonance (NMR) spectra via comparison of the integral of the methyl protons originating from the ethyl carbonate side chain on the PGC segment resonating at 1.1−1.2 ppm with that of methyl protons from CPT at 0.91 ppm (Figures S7−S9 and S11). All polymers were rigorously characterized by ^{1}H NMR, ^{13}C NMR, Fourier-transform infrared spectroscopy (FT-IR), thermogravimetric analysis (TGA), and differential scanning calorimetry (DSC) (Figures S2−S15).

Polymer assemblies (0.5 mg/mL) were prepared by nanoprecipitation from DMSO into nanopure water and then dialyzed against nanopure water for 24 h to remove organic solvent. The number-average hydrodynamic diameters ($D_{h(number)}$) of the polymer nanoconstructs were in the range 20−50 nm (Figure 1). Transmission electron microscopy (TEM) and atomic force microscopy (AFM) analyses of polymer nanoparticles showed globular structures with average diameters in agreement with those obtained from dynamic light scattering (DLS), independent of f_{CPT}.

However, polymer **3** assemblies exhibited significant f_{CPT}-dependent heights and diameter-to-height (D/H) ratios, with number-average heights ranging from 2 to 10 nm and D/H ratios ranging from 4 to 26 (Figure 1). At low CPT conjugation levels, the polymer assemblies exhibited significantly lower heights and greater D/H ratios, with f_{CPT} of 0 and 0.15 having heights that were ca. 4−5-fold lower and D/H ratios that were ca. 4−6-fold higher than those of the polymer assemblies with f_{CPT} of 0.50 and 0.85. These AFM data indicated that the nanomaterials with lower f_{CPT} deformed to a greater extent upon drop deposition from aqueous solution onto the polar mica substrate, suggesting

https://dx.doi.org/10.1021/acs.nanolett.0c02319
Nano Lett. 2020, 20, 6563−6571

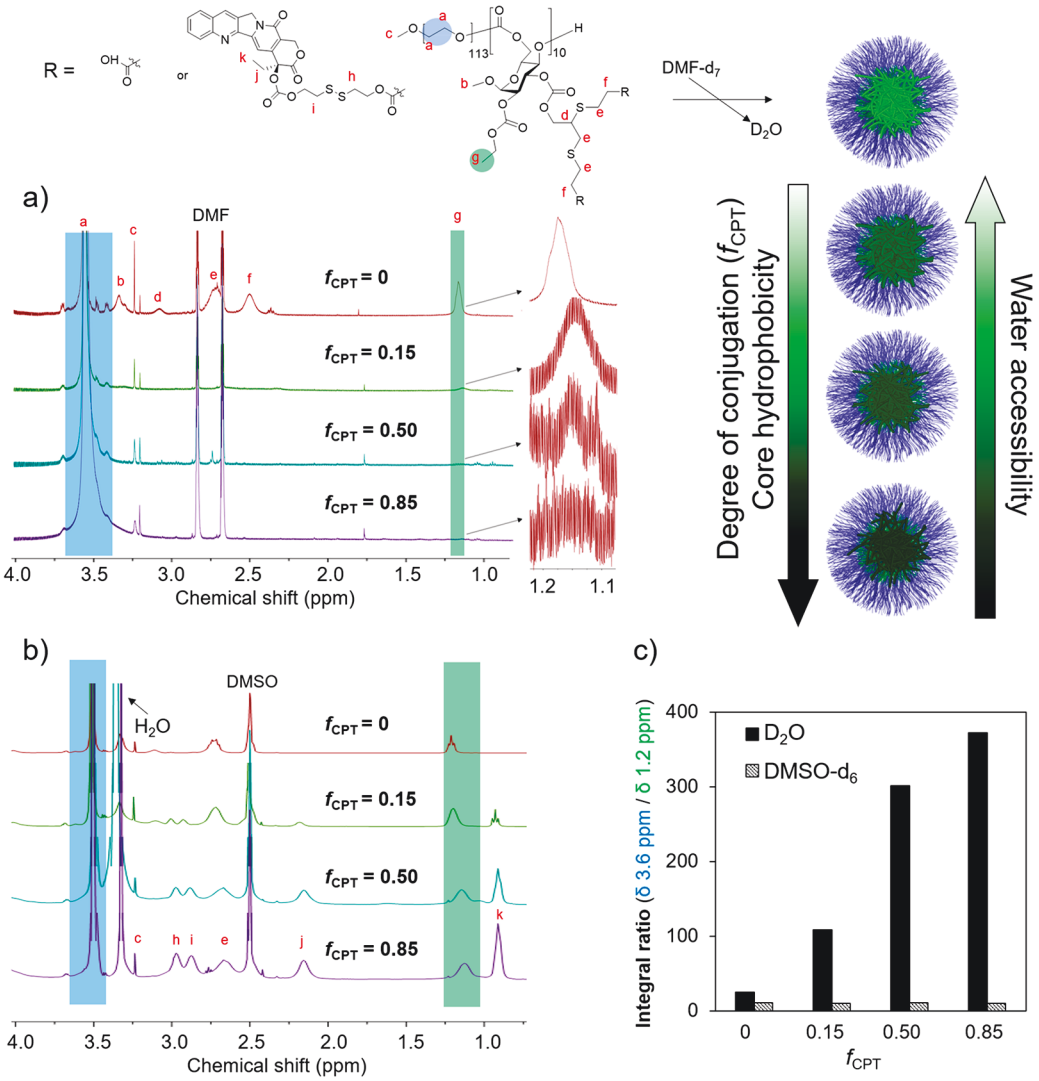

Figure 2. (a) ^{1}H NMR spectra for the assemblies from polymers **2** and **3** in D_2O, highlighting the PEG methylene proton resonance (δ 3.6 ppm, blue) and the PGC ethyl carbonate methyl proton resonance (δ 1.2−1.1 ppm, green). (b) ^{1}H NMR spectra for polymers **2** and **3** in DMSO-d_6. (c) Integral ratios (δ 3.6 ppm/δ 1.2−1.1 ppm) in D_2O vs DMSO-d_6.

greater water plasticization of the nanostructures. In contrast, the higher f_{CPT} counterparts remained as stable, globular structures (Figure 1), suggesting greater rigidity provided by exclusion of water from the more hydrophobic core domains.

As a measure of the local microenvironment within the polymer nanoassemblies, solution-state ^{1}H NMR spectroscopy was employed to monitor the mobility of the PGC chain segments when packaged within nanoassemblies in D_2O vs as solvated polymer chains in DMSO-d_6, confirming that higher f_{CPT} led to lower water accessibility. The previous literature has reported the importance of the microenvironment adjacent to disulfide bonds for controlling the thiol−disulfide exchange kinetics.[43,44] The NMR signal corresponding to the PGC ethyl carbonate methyl proton resonance (i.e., 1.2 ppm, highlighted in green in Figure 2) was utilized to probe the microenvironment adjacent to the disulfide-linkages in the assembly core. Poor solvation of the relatively hydrophobic PGC segment in the aqueous environment was made evident by the reduction of intensity and broadening of the PGC-associated proton resonances in D_2O, in comparison to protons of the PEG segments (Figure 2a). This phenomenon was quantified by the ratio of the ^{1}H NMR integrations between PEG-associated protons resonating at 3.6 ppm and PGC-associated protons resonating at 1.2 ppm (Figure 2c). The relative change in NMR signal intensity provides insights into the molecular microenvironment. As f_{CPT} increased from 0 to 0.85, the integral ratio (δ 3.6 ppm/δ 1.2 ppm) underwent an ca. 15-fold increase from 25 to 372 in D_2O, indicating reduced solvation of the disulfide-containing PGC segment in aqueous media (Figure 2c). At $f_{CPT} \geq 0.50$, minimal proton resonances from CPT and PGC were observed in the ^{1}H NMR spectra, indicating reduced chain mobility caused by limited aqueous accessibility. CPT influenced the chemical shifts of the methyl protons, presumably due to intramolecular van der Waals interactions, resulting in a slight upfield shift of the PGC ethyl carbonate methyl proton resonance as f_{CPT} increased (Figure 2b).[66−68] The integral ratio (δ 3.6 ppm/δ 1.2−1.1 ppm) remained constant at ca. 11 when any of the four polymers was solvated in DMSO-d_6 (Figure 2b,c) independent of f_{CPT}. The lack of change for proton relaxation in DMSO-d_6 verified that the integral ratio changes in D_2O were due to differential solvation between PEG and PGC segments with a lower aqueous accessibility of the core-forming sugar segment (Figure 2).

https://dx.doi.org/10.1021/acs.nanolett.0c02319
Nano Lett. 2020, 20, 6563−6571

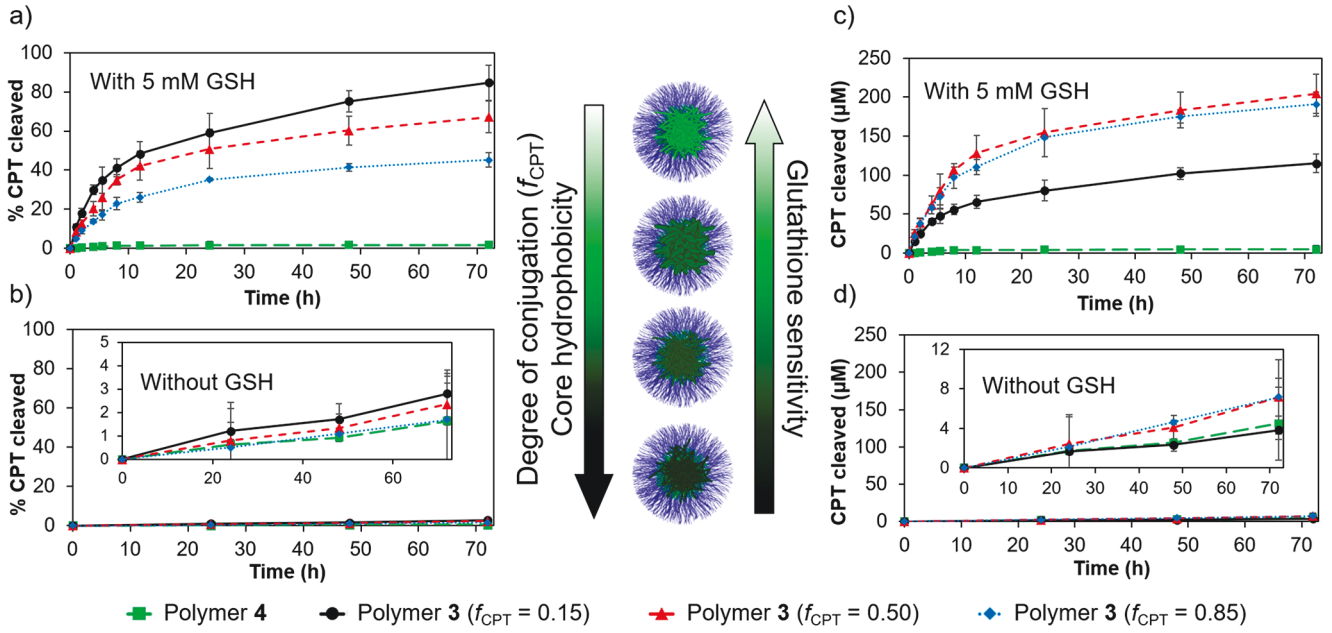

Figure 3. Disulfide cleavages and drug releases of CPT-conjugated polymer nanomaterials (0.5 mg/mL, 2 mL) studied over 3 days at 37 °C in PBS buffer (pH 7.4) in triplicate (a, c) with 5 mM GSH and (b, d) without GSH. The results are presented as (a, b) % CPT release and (c, d) CPT molar release.

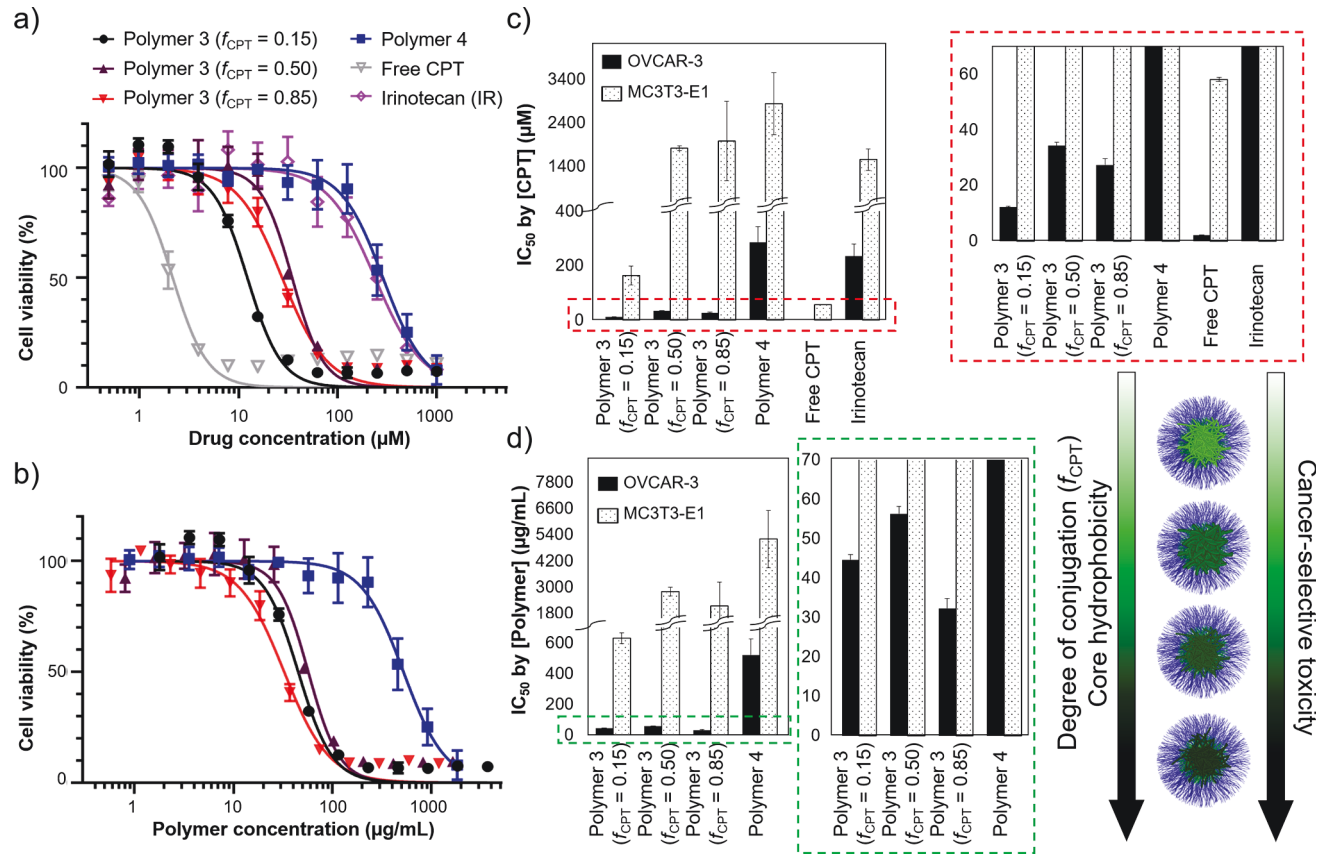

Figure 4. Cytotoxicity evaluation of CPT-conjugated polymers in OVCAR-3 ovarian cancer cells based on (a) CPT concentrations or (b) polymer concentrations. (c) Half maximal inhibitory concentration (IC_{50}) obtained from the data plotted in part a, with the red dashed box showing a zoom-in view. (d) IC_{50} obtained from the data plotted in part b, with the green dashed box showing a zoom-in view. Cell viabilities are reported as an average of three measurements, and error bars represent standard deviation.

The higher aqueous accessibility led to an increase in the GSH sensitivity, as revealed by disulfide cleavage experiments in PBS solutions (pH = 7.4) at 37 °C in the presence of GSH (5 mM) as a function of time (Figure 3). Calculations of the % disulfide cleavage were based on the free CPT concentrations in aliquots collected at predetermined time points using high-performance

https://dx.doi.org/10.1021/acs.nanolett.0c02319
Nano Lett. 2020, 20, 6563−6571

liquid chromatography (HPLC).[69] CPT was released from polymer **3** assemblies upon exposure to GSH, with an initial rapid release followed by sustained release (Figure 3a,c). Higher f_{CPT} led to slower GSH-triggered disulfide cleavage and CPT release. In the presence of 5 mM GSH, polymer **3** assemblies underwent 30%, 20%, and 14% of the total CPT release in the first 4 h with f_{CPT} of 0.15, 0.50, and 0.85, respectively. After 72 h, polymer **3** assemblies with f_{CPT} of 0.15, 0.50, and 0.85 had released 85%, 67%, and 45% of the total CPT, respectively (Figure 3a). Although the lowest f_{CPT} of 0.15 achieved the fastest and greatest % CPT release, it resulted in the lowest CPT concentration due to the limited overall amount of drug loaded (Figure 3c and Table S1). As expected, minimal disulfide cleavage occurred in samples without GSH (Figure 3b,d). As control studies, assemblies of non-redox-responsive CPT-conjugated polymer **4** exhibited minimal CPT release with or without GSH over a period of 72 h (Figure 3). Interestingly, polymer **3** assemblies with f_{CPT} of 0.85 exhibited a similar CPT release profile in comparison to the f_{CPT} of the 0.50 counterpart (Figure 3c,d), despite a greater drug loading that resulted in a higher total amount of loaded CPT at the same 0.5 mg/mL polymer concentration (Table S1). This phenomenon can be explained as a result of a slower GSH-triggered drug release from nanoparticles with a higher f_{CPT}. These findings indicate that a higher conjugation of hydrophobic drug led to a lower stimuli-responsive sensitivity against water-soluble stimuli (e.g., GSH).

The GSH sensitivity was also shown to significantly influence the *in vitro* cytotoxicities of the redox-responsive CPT-conjugated nanomaterials against OVCAR-3 ovarian cancer cells (Figure 4 and Table S2). Ovarian cancer is the most lethal gynecological cancer in the Western world, with ca. 75% cases that were diagnosed at late stages (III/IV) having a 5 year survival rate <50%.[70] The polymer **3** with f_{CPT} of 0.15 was most efficacious against cancer cells with the lowest IC_{50} value (12 μM) in comparison to f_{CPT} of 0.50 (IC_{50} = 34 μM) and f_{CPT} of 0.85 (IC_{50} = 27 μM) counterparts (Figure 4). When IC_{50} values were determined based on polymer concentrations, rather than CPT concentrations, polymer **3** with the highest f_{CPT} of 0.85 displayed the lowest IC_{50} value, i.e., the highest cytotoxicity against OVCAR-3 cancer cells (Figure 4b and Table S2). The observed *in vitro* outcomes can be attributed to the complex interplay between nanocarriers and the environment; higher hydrophobic payload reduced diffusion of GSH into and free CPT out from the nanoparticle assemblies, thereby affecting disulfide cleavage and the resulting CPT release kinetics. Moreover, differences in f_{CPT} for the initial polymer chains, and the changing levels of f_{CPT} during CPT cleavage, each could contribute to variations in the polymer chain hydrophilicity, thereby affecting the packing parameters and potentially leading to variable extents of polymer chain assembly and disassembly. Therefore, additional factors, such as slight differences in size, morphologies, and polymer chain packings, could profoundly impact the *in vitro* outcomes. The disulfide-linked CPT-conjugated polymer **3** assemblies displayed reduced cytotoxicities over the free CPT (IC_{50} = 2.1 μM), partly due to a sustained release of CPT, where even after 3 days, polymer **3** assemblies with f_{CPT} of 0.15, 0.50, and 0.85 only cleaved 85%, 67%, and 45% of the total conjugated CPT in the presence of 5 mM GSH in PBS, respectively (Figure 3a). Although having high *in vitro* cytotoxicities, free CPT has poor aqueous solubility and causes severe side effects that have resulted in limited clinical usage.[71] Polymers **3** displayed a significantly higher cytotoxicity while maintaining good water solubility when compared to irinotecan (IR, IC_{50} = 236 μM), a water-soluble CPT analogue that has received FDA-approval for treating colorectal cancers and has been investigated as a candidate for ovarian cancers in clinical trials.[71−74] Furthermore, the GSH-responsive CPT-conjugated polymers **3** were 1 order of magnitude more efficacious against ovarian cancer cells in comparison to the nonresponsive CPT-conjugated polymer **4** (IC_{50} = 287 μM), demonstrating the essential role of the redox-responsive disulfide-linkages in maintaining drug efficacy. It is worth noting that polymer **2** (f_{CPT} = 0) was noncytotoxic at the tested concentration ranges (16−2000 μg/mL, Figure S16).

We further investigated the effect of GSH sensitivity of the redox-responsive CPT-conjugated nanomaterials on the differential cytotoxicity between cancerous and healthy cells (Figure 4 and Figure S17). Although chemotherapeutic agents help combat cancers, off-site toxicities for healthy tissues cause adverse effects; for instance, toxicity against bone marrow increases the risks of developing hypoplastic anemia and myelodysplastic syndrome.[75−77] Osteoblasts regulate hematopoietic stem cell niches and are essential for the hematopoietic cell repopulation after chemotherapies.[78] Therefore, the ideal anticancer agents should spare osteoblasts while attacking cancer cells. For this reason, OVCAR-3 ovarian cancer cells and MC3T3-E1 osteoblast progenitor cells were selected to represent cancerous and healthy cells, respectively. The selectivity was calculated as the ratio of the IC_{50} values against noncancerous MC3T3-E1 vs cancerous OVCAR-3 ($IC_{50\text{-}(MC3T3\text{-}E1)}/IC_{50\text{-}(OVCAR\text{-}3)}$) in order to quantify the differential cytotoxicity. A higher selectivity value ($IC_{50\text{-}(MC3T3\text{-}E1)}/IC_{50\text{-}(OVCAR\text{-}3)}$) suggests a wider therapeutic window for the formulation. Polymers **3** with f_{CPT} of 0.15, 0.50, and 0.85 had selectivity values of 13, 53, and 72, respectively: higher than those of nonresponsive polymer **4** (selectivity value = 10) and IR (selectivity value = 7) formulations (Figure 4 and Figure S17 and Table S2), indicating a better safety profile for the GSH-responsive CPT-conjugated nanomaterials. The differential cytotoxicities of polymer **3** assemblies possibly arose from higher GSH concentrations in cancer cells vs healthy cells.[24,27] A similar trend was observed among polymer **3** assemblies when selectivity values were calculated based on polymer concentrations: a higher f_{CPT} led to a greater cancer-selective cytotoxicity (Figure S18). Although the highest f_{CPT} of 0.85 resulted in reduced cytotoxicity, it led to a ca. 5.5-fold increase in the differential cytotoxicity against ovarian cancer cells in comparison to the f_{CPT} of the 0.15 counterpart (Figure 4, Figure S18 and Table S2). The differences in GSH sensitivities resulted in significant variations in the cancer selectivity, demonstrating the importance of controlling the stimuli sensitivity of smart drug carriers. With the improved differential cytotoxicity, our redox-responsive CPT-conjugated sugar-based polymeric nanomaterials showed great promise for treating ovarian cancers and associated metastatic diseases.

In summary, we demonstrated the impact of hydrophobic drug conjugation on the complex interplay between the level of drug loading on the polymer nanoparticle physicochemical characteristics and the resulting access of molecular stimuli to the internal compartments and subsequent triggered drug release, with a focus on GSH sensitivity of disulfide-linked CPT-conjugated PEG-*b*-PGC nanomaterials. The hydrophobic payload increased the core hydrophobicity, which negatively influenced the aqueous accessibility, lowered the GSH sensitivity, and consequently slowed down the GSH-triggered drug release. Importantly, when compared to the low CPT

https://dx.doi.org/10.1021/acs.nanolett.0c02319
Nano Lett. 2020, 20, 6563−6571

loading formulation (f_{CPT} = 0.15), the higher CPT-conjugated formulations (f_{CPT} = 0.50 and 0.85) significantly improved selective cytotoxicities against ovarian cancer cells over healthy cells. With an emphasis on the importance of controlling the drug loading, this work represents a significant advancement in the drug carrier design, providing a versatile strategy to tune GSH sensitivity through payload control, with the potential for extending this strategy to other water-borne stimuli, including enzymes, peptides, pH, and other ions.

■ ASSOCIATED CONTENT

Supporting Information

The Supporting Information is available free of charge at https://pubs.acs.org/doi/10.1021/acs.nanolett.0c02319.

Experimental details regarding materials, instrumentation, methods, and full physicochemical and biological characterization data (PDF)

■ AUTHOR INFORMATION

Corresponding Authors

Fuwu Zhang − *Departments of Chemistry, Chemical Engineering, and Materials Science & Engineering, Laboratory for Synthetic−Biologic Interactions, Texas A&M University, College Station, Texas 77842, United States;* orcid.org/0000-0002-1928-3472; Email: zhangfuwu1314@gmail.com

Karen L. Wooley − *Departments of Chemistry, Chemical Engineering, and Materials Science & Engineering, Laboratory for Synthetic−Biologic Interactions, Texas A&M University, College Station, Texas 77842, United States;* orcid.org/0000-0003-4086-384X; Email: wooley@chem.tamu.edu

Authors

Yen-Nan Lin − *Departments of Chemistry, Chemical Engineering, and Materials Science & Engineering, Laboratory for Synthetic−Biologic Interactions and College of Medicine, Texas A&M University, College Station, Texas 77842, United States;* orcid.org/0000-0001-7118-7771

Sarosh Khan − *Departments of Chemistry, Chemical Engineering, and Materials Science & Engineering, Laboratory for Synthetic−Biologic Interactions, Texas A&M University, College Station, Texas 77842, United States*

Yue Song − *Departments of Chemistry, Chemical Engineering, and Materials Science & Engineering, Laboratory for Synthetic−Biologic Interactions, Texas A&M University, College Station, Texas 77842, United States;* orcid.org/0000-0002-7800-5528

Mei Dong − *Departments of Chemistry, Chemical Engineering, and Materials Science & Engineering, Laboratory for Synthetic−Biologic Interactions, Texas A&M University, College Station, Texas 77842, United States;* orcid.org/0000-0002-9862-0296

Yidan Shen − *Departments of Chemistry, Chemical Engineering, and Materials Science & Engineering, Laboratory for Synthetic−Biologic Interactions, Texas A&M University, College Station, Texas 77842, United States*

David K. Tran − *Departments of Chemistry, Chemical Engineering, and Materials Science & Engineering, Laboratory for Synthetic−Biologic Interactions, Texas A&M University, College Station, Texas 77842, United States;* orcid.org/0000-0002-4877-166X

Ching Pang − *Departments of Chemistry, Chemical Engineering, and Materials Science & Engineering, Laboratory for Synthetic−Biologic Interactions, Texas A&M University, College Station, Texas 77842, United States;* orcid.org/0000-0002-4497-7898

Complete contact information is available at: https://pubs.acs.org/10.1021/acs.nanolett.0c02319

Notes

The authors declare no competing financial interest.

■ ACKNOWLEDGMENTS

We gratefully acknowledge financial support from the National Science Foundation (CHE-1610311, CHE-2003771, DMR-1905818, and DMREF-1629094), and the Robert A. Welch Foundation through the W. T. Doherty-Welch Chair in Chemistry (A-0001). The Laboratory for Synthetic-Biologic Interactions (LSBI) at Texas A&M University is also acknowledged.

■ REFERENCES

(1) McRae Page, S.; Martorella, M.; Parelkar, S.; Kosif, I.; Emrick, T. Disulfide Cross-Linked Phosphorylcholine Micelles for Triggered Release of Camptothecin. *Mol. Pharmaceutics* **2013**, *10* (7), 2684−2692.

(2) Wang, B.; Ding, Y.; Zhao, X.; Han, X.; Yang, N.; Zhang, Y.; Zhao, Y.; Zhao, X.; Taleb, M.; Miao, Q. R.; Nie, G. Delivery of small interfering RNA against Nogo-B receptor *via* tumor-acidity responsive nanoparticles for tumor vessel normalization and metastasis suppression. *Biomaterials* **2018**, *175*, 110−122.

(3) Sun, H.; Yan, L.; Chang, M. Y. Z.; Carter, K. A.; Zhang, R.; Slyker, L.; Lovell, J. F.; Wu, Y.; Cheng, C. A multifunctional biodegradable brush polymer-drug conjugate for paclitaxel/gemcitabine co-delivery and tumor imaging. *Nanoscale Adv.* **2019**, *1* (7), 2761−2771.

(4) Meng, F.; Wang, J.; Ping, Q.; Yeo, Y. Camouflaging Nanoparticles for Ratiometric Delivery of Therapeutic Combinations. *Nano Lett.* **2019**, *19* (3), 1479−1487.

(5) Saw, P. E.; Yao, H.; Lin, C.; Tao, W.; Farokhzad, O. C.; Xu, X. Stimuli-Responsive Polymer−Prodrug Hybrid Nanoplatform for Multistage siRNA Delivery and Combination Cancer Therapy. *Nano Lett.* **2019**, *19* (9), 5967−5974.

(6) Lin, Y.-N.; Elsabahy, M.; Khan, S.; Zhang, F.; Song, Y.; Dong, M.; Li, R.; Smolen, J.; Letteri, R. A.; Su, L.; Wooley, K. L. Erythrocyte-Membrane-Camouflaged Nanocarriers with Tunable Paclitaxel Release Kinetics *via* Macromolecular Stereocomplexation. *ACS Mater. Lett.* **2020**, *2*, 595−601.

(7) Qin, H.; Ding, Y.; Mujeeb, A.; Zhao, Y.; Nie, G. Tumor Microenvironment Targeting and Responsive Peptide-Based Nanoformulations for Improved Tumor Therapy. *Mol. Pharmacol.* **2017**, *92* (3), 219−231.

(8) Chen, X.; Zhou, W.; Liang, C.; Shi, S.; Yu, X.; Chen, Q.; Sun, T.; Lu, Y.; Zhang, Y.; Guo, Q.; Li, C.; Zhang, Y.; Jiang, C. Codelivery Nanosystem Targeting the Deep Microenvironment of Pancreatic Cancer. *Nano Lett.* **2019**, *19* (6), 3527−3534.

(9) Banskota, S.; Saha, S.; Bhattacharya, J.; Kirmani, N.; Yousefpour, P.; Dzuricky, M.; Zakharov, N.; Li, X.; Spasojevic, I.; Young, K.; Chilkoti, A. Genetically Encoded Stealth Nanoparticles of a Zwitterionic Polypeptide-Paclitaxel Conjugate Have a Wider Therapeutic Window than Abraxane in Multiple Tumor Models. *Nano Lett.* **2020**, *20* (4), 2396−2409.

(10) Parrish, B.; Emrick, T. Soluble Camptothecin Derivatives Prepared by Click Cycloaddition Chemistry on Functional Aliphatic Polyesters. *Bioconjugate Chem.* **2007**, *18* (1), 263−267.

(11) Su, L.; Li, R.; Khan, S.; Clanton, R.; Zhang, F.; Lin, Y.-N.; Song, Y.; Wang, H.; Fan, J.; Hernandez, S.; Butters, A. S.; Akabani, G.; MacLoughlin, R.; Smolen, J.; Wooley, K. L. Chemical Design of Both a Glutathione-Sensitive Dimeric Drug Guest and a Glucose-Derived Nanocarrier Host to Achieve Enhanced Osteosarcoma Lung Metastatic Anticancer Selectivity. *J. Am. Chem. Soc.* **2018**, *140* (4), 1438−1446.

(12) Yang, C.; Tan, J. P. K.; Cheng, W.; Attia, A. B. E.; Ting, C. T. Y.; Nelson, A.; Hedrick, J. L.; Yang, Y.-Y. Supramolecular nanostructures designed for high cargo loading capacity and kinetic stability. *Nano Today* **2010**, *5* (6), 515−523.
(13) Samarajeewa, S.; Shrestha, R.; Elsabahy, M.; Karwa, A.; Li, A.; Zentay, R. P.; Kostelc, J. G.; Dorshow, R. B.; Wooley, K. L. *In Vitro* Efficacy of Paclitaxel-Loaded Dual-Responsive Shell Cross-Linked Polymer Nanoparticles Having Orthogonally Degradable Disulfide Cross-Linked Corona and Polyester Core Domains. *Mol. Pharmaceutics* **2013**, *10* (3), 1092−1099.
(14) Lv, S.; Wu, Y.; Cai, K.; He, H.; Li, Y.; Lan, M.; Chen, X.; Cheng, J.; Yin, L. High Drug Loading and Sub-Quantitative Loading Efficiency of Polymeric Micelles Driven by Donor-Receptor Coordination Interactions. *J. Am. Chem. Soc.* **2018**, *140* (4), 1235−1238.
(15) Ansari, M.; Moradi, S.; Shahlaei, M. A molecular dynamics simulation study on the mechanism of loading of gemcitabine and camptothecin in poly lactic-co-glycolic acid as a nano drug delivery system. *J. Mol. Liq.* **2018**, *269*, 110−118.
(16) Jafari, A.; Yan, L.; Mohamed, M. A.; Wu, Y.; Cheng, C. Well-Defined Diblock Poly(ethylene glycol)-b-Poly(ε-caprolactone)-Based Polymer-Drug Conjugate Micelles for pH-Responsive Delivery of Doxorubicin. *Materials* **2020**, *13* (7), 1510.
(17) Elsabahy, M.; Wooley, K. L. Design of polymeric nanoparticles for biomedical delivery applications. *Chem. Soc. Rev.* **2012**, *41* (7), 2545−2561.
(18) Champion, J. A.; Mitragotri, S. Role of target geometry in phagocytosis. *Proc. Natl. Acad. Sci. U. S. A.* **2006**, *103* (13), 4930−4934.
(19) Geng, Y.; Dalhaimer, P.; Cai, S.; Tsai, R.; Tewari, M.; Minko, T.; Discher, D. E. Shape effects of filaments versus spherical particles in flow and drug delivery. *Nat. Nanotechnol.* **2007**, *2* (4), 249−255.
(20) Petros, R. A.; DeSimone, J. M. Strategies in the design of nanoparticles for therapeutic applications. *Nat. Rev. Drug Discovery* **2010**, *9* (8), 615−627.
(21) Sun, T.; Zhang, Y. S.; Pang, B.; Hyun, D. C.; Yang, M.; Xia, Y. Engineered Nanoparticles for Drug Delivery in Cancer Therapy. *Angew. Chem., Int. Ed.* **2014**, *53* (46), 12320−12364.
(22) Cheng, K.; Ding, Y.; Zhao, Y.; Ye, S.; Zhao, X.; Zhang, Y.; Ji, T.; Wu, H.; Wang, B.; Anderson, G. J.; Ren, L.; Nie, G. Sequentially Responsive Therapeutic Peptide Assembling Nanoparticles for Dual-Targeted Cancer Immunotherapy. *Nano Lett.* **2018**, *18* (5), 3250−3258.
(23) Mohamed, M. A.; Fallahi, A.; El-Sokkary, A. M. A.; Salehi, S.; Akl, M. A.; Jafari, A.; Tamayol, A.; Fenniri, H.; Khademhosseini, A.; Andreadis, S. T.; Cheng, C. Stimuli-responsive hydrogels for manipulation of cell microenvironment: From chemistry to biofabrication technology. *Prog. Polym. Sci.* **2019**, *98*, 101147.
(24) Russo, A.; DeGraff, W.; Friedman, N.; Mitchell, J. B. Selective Modulation of Glutathione Levels in Human Normal versus Tumor Cells and Subsequent Differential Response to Chemotherapy Drugs. *Cancer Res.* **1986**, *46* (6), 2845−2848.
(25) Raina, S.; Missiakas, D. Making and Breaking Disulfide Bonds. *Annu. Rev. Microbiol.* **1997**, *51* (1), 179−202.
(26) Schafer, F. Q.; Buettner, G. R. Redox environment of the cell as viewed through the redox state of the glutathione disulfide/glutathione couple. *Free Radical Biol. Med.* **2001**, *30* (11), 1191−1212.
(27) Kuppusamy, P.; Li, H.; Ilangovan, G.; Cardounel, A. J.; Zweier, J. L.; Yamada, K.; Krishna, M. C.; Mitchell, J. B. Noninvasive Imaging of Tumor Redox Status and Its Modification by Tissue Glutathione Levels. *Cancer Res.* **2002**, *62* (1), 307−312.
(28) Saito, G.; Swanson, J. A.; Lee, K.-D. Drug delivery strategy utilizing conjugation *via* reversible disulfide-linkages: role and site of cellular reducing activities. *Adv. Drug Delivery Rev.* **2003**, *55* (2), 199−215.
(29) Liu, J.; Pang, Y.; Huang, W.; Huang, X.; Meng, L.; Zhu, X.; Zhou, Y.; Yan, D. Bioreducible Micelles Self-Assembled from Amphiphilic Hyperbranched Multiarm Copolymer for Glutathione-Mediated Intracellular Drug Delivery. *Biomacromolecules* **2011**, *12* (5), 1567−1577.
(30) Bajpai, A. K.; Shukla, S. K.; Bhanu, S.; Kankane, S. Responsive polymers in controlled drug delivery. *Prog. Polym. Sci.* **2008**, *33* (11), 1088−1118.
(31) Zhang, W.; Lin, W.; Zheng, X.; He, S.; Xie, Z. Comparing Effects of Redox Sensitivity of Organic Nanoparticles to Photodynamic Activity. *Chem. Mater.* **2017**, *29* (4), 1856−1863.
(32) Thorpe, P. E.; Wallace, P. M.; Knowles, P. P.; Relf, M. G.; Brown, A. N. F.; Watson, G. J.; Knyba, R. E.; Wawrzynczak, E. J.; Blakey, D. C. New Coupling Agents for the Synthesis of Immunotoxins Containing a Hindered Disulfide Bond with Improved Stability *In Vivo*. *Cancer Res.* **1987**, *47* (22), 5924−5931.
(33) Arpicco, S.; Dosio, F.; Brusa, P.; Crosasso, P.; Cattel, L. New Coupling Reagents for the Preparation of Disulfide Cross-Linked Conjugates with Increased Stability. *Bioconjugate Chem.* **1997**, *8* (3), 327−337.
(34) Kellogg, B. A.; Garrett, L.; Kovtun, Y.; Lai, K. C.; Leece, B.; Miller, M.; Payne, G.; Steeves, R.; Whiteman, K. R.; Widdison, W.; Xie, H.; Singh, R.; Chari, R. V. J.; Lambert, J. M.; Lutz, R. J. Disulfide-Linked Antibody-Maytansinoid Conjugates: Optimization of *In Vivo* Activity by Varying the Steric Hindrance at Carbon Atoms Adjacent to the Disulfide Linkage. *Bioconjugate Chem.* **2011**, *22* (4), 717−727.
(35) Zhai, L.; Liang, J.; Guo, X.; Zhao, Y.; Wu, C. Extraordinary Modulation of Disulfide Redox-Responsiveness by Cooperativity of Twin-Disulfide Bonds. *Chem. - Eur. J.* **2014**, *20* (52), 17507−17514.
(36) Mirzahosseini, A.; Noszál, B. Species-specific thiol-disulfide equilibrium constants of ovothiol A and penicillamine with glutathione. *RSC Adv.* **2016**, *6* (32), 26757−26764.
(37) Liu, J.; Pang, Y.; Huang, W.; Zhu, Z.; Zhu, X.; Zhou, Y.; Yan, D. Redox-Responsive Polyphosphate Nanosized Assemblies: A Smart Drug Delivery Platform for Cancer Therapy. *Biomacromolecules* **2011**, *12* (6), 2407−2415.
(38) Zhang, F.; Zhu, G.; Jacobson, O.; Liu, Y.; Chen, K.; Yu, G.; Ni, Q.; Fan, J.; Yang, Z.; Xu, F.; Fu, X.; Wang, Z.; Ma, Y.; Niu, G.; Zhao, X.; Chen, X. Transformative Nanomedicine of an Amphiphilic Camptothecin Prodrug for Long Circulation and High Tumor Uptake in Cancer Therapy. *ACS Nano* **2017**, *11* (9), 8838−8848.
(39) Tang, L.; Yu, F.; Tang, B.; Yang, Z.; Fan, W.; Zhang, M.; Wang, Z.; Jacobson, O.; Zhou, Z.; Li, L.; Liu, Y.; Kiesewetter, D. O.; Tang, W.; He, L.; Ma, Y.; Niu, G.; Zhang, X.; Chen, X. Tumor Microenvironment-Activated Ultrasensitive Nanoprobes for Specific Detection of Intratumoral Glutathione by Ratiometric Photoacoustic Imaging. *ACS Appl. Mater. Interfaces* **2019**, *11* (31), 27558−27567.
(40) Wang, D.; Jin, Y.; Zhu, X.; Yan, D. Synthesis and applications of stimuli-responsive hyperbranched polymers. *Prog. Polym. Sci.* **2017**, *64*, 114−153.
(41) Li, Y.; Wu, Y.; Chen, J.; Wan, J.; Xiao, C.; Guan, J.; Song, X.; Li, S.; Zhang, M.; Cui, H.; Li, T.; Yang, X.; Li, Z.; Yang, X. A Simple Glutathione-Responsive Turn-On Theranostic Nanoparticle for Dual-Modal Imaging and Chemo-Photothermal Combination Therapy. *Nano Lett.* **2019**, *19* (8), 5806−5817.
(42) Cheng, R.; Feng, F.; Meng, F.; Deng, C.; Feijen, J.; Zhong, Z. Glutathione-responsive nano-vehicles as a promising platform for targeted intracellular drug and gene delivery. *J. Controlled Release* **2011**, *152* (1), 2−12.
(43) Wu, C.; Belenda, C.; Leroux, J.-C.; Gauthier, M. A. Interplay of Chemical Microenvironment and Redox Environment on Thiol-Disulfide Exchange Kinetics. *Chem. - Eur. J.* **2011**, *17* (36), 10064−10070.
(44) Wu, C.; Wang, S.; Brülisauer, L.; Leroux, J.-C.; Gauthier, M. A. Broad Control of Disulfide Stability through Microenvironmental Effects and Analysis in Complex Redox Environments. *Biomacromolecules* **2013**, *14* (7), 2383−2388.
(45) Zhuang, J.; Zhao, B.; Thayumanavan, S. Cascaded Step-Growth Polymerization for Functional Polyamides with Diverse Architectures and Stimuli Responsive Characteristics. *ACS Macro Lett.* **2019**, *8* (3), 245−249.
(46) Jiang, Z.; Thayumanavan, S. Disulfide-Containing Macromolecules for Therapeutic Delivery. *Isr. J. Chem.* **2020**, *60* (1−2), 132−139.

https://dx.doi.org/10.1021/acs.nanolett.0c02319
Nano Lett. 2020, 20, 6563−6571

(47) Yao, Y.; Xu, H.; Liu, C.; Guan, Y.; Xu, D.; Zhang, J.; Su, Y.; Zhao, L.; Luo, J. Biodegradable multi-blocked polyurethane micelles for intracellular drug delivery: the effect of disulfide location on the drug release profile. *RSC Adv.* **2016**, *6* (11), 9082−9089.
(48) Chan, N.; An, S. Y.; Oh, J. K. Dual location disulfide degradable interlayer-crosslinked micelles with extended sheddable coronas exhibiting enhanced colloidal stability and rapid release. *Polym. Chem.* **2014**, *5* (5), 1637−1649.
(49) Ghosh, S.; Basu, S.; Thayumanavan, S. Simultaneous and Reversible Functionalization of Copolymers for Biological Applications. *Macromolecules* **2006**, *39* (17), 5595−5597.
(50) Ryu, J.-H.; Chacko, R. T.; Jiwpanich, S.; Bickerton, S.; Babu, R. P.; Thayumanavan, S. Self-Cross-Linked Polymer Nanogels: A Versatile Nanoscopic Drug Delivery Platform. *J. Am. Chem. Soc.* **2010**, *132* (48), 17227−17235.
(51) Ryu, J.-H.; Jiwpanich, S.; Chacko, R.; Bickerton, S.; Thayumanavan, S. Surface-Functionalizable Polymer Nanogels with Facile Hydrophobic Guest Encapsulation Capabilities. *J. Am. Chem. Soc.* **2010**, *132* (24), 8246−8247.
(52) Zhuang, J.; Chacko, R.; Amado Torres, D. F.; Wang, H.; Thayumanavan, S. Dual Stimuli-Dual Response Nanoassemblies Prepared from a Simple Homopolymer. *ACS Macro Lett.* **2014**, *3* (1), 1−5.
(53) Xu, H.; Cao, W.; Zhang, X. Selenium-Containing Polymers: Promising Biomaterials for Controlled Release and Enzyme Mimics. *Acc. Chem. Res.* **2013**, *46* (7), 1647−1658.
(54) Cao, W.; Wang, L.; Xu, H. Selenium/tellurium containing polymer materials in nanobiotechnology. *Nano Today* **2015**, *10* (6), 717−736.
(55) Nuttall, K. L. Evaluating selenium poisoning. *Ann. Clin. Lab. Sci.* **2006**, *36* (4), 409−420.
(56) Vinceti, M.; Mandrioli, J.; Borella, P.; Michalke, B.; Tsatsakis, A.; Finkelstein, Y. Selenium neurotoxicity in humans: Bridging laboratory and epidemiologic studies. *Toxicol. Lett.* **2014**, *230* (2), 295−303.
(57) Rae, W.; Kitley, J.; Pinto, A. Selenium Toxicity Associated With Reversible Leukoencephalopathy and Cortical Blindness. *JAMA Neurol.* **2018**, *75* (10), 1282−1283.
(58) Chen, X.; McRae, S.; Parelkar, S.; Emrick, T. Polymeric Phosphorylcholine-Camptothecin Conjugates Prepared by Controlled Free Radical Polymerization and Click Chemistry. *Bioconjugate Chem.* **2009**, *20* (12), 2331−2341.
(59) Xu, Z.; Wang, D.; Xu, S.; Liu, X.; Zhang, X.; Zhang, H. Preparation of a Camptothecin Prodrug with Glutathione-Responsive Disulfide Linker for Anticancer Drug Delivery. *Chem. - Asian J.* **2014**, *9* (1), 199−205.
(60) Zhang, Q.; He, J.; Zhang, M.; Ni, P. A polyphosphoester-conjugated camptothecin prodrug with disulfide linkage for potent reduction-triggered drug delivery. *J. Mater. Chem. B* **2015**, *3* (24), 4922−4932.
(61) Li, J.; Li, Y.; Wang, Y.; Ke, W.; Chen, W.; Wang, W.; Ge, Z. Polymer Prodrug-Based Nanoreactors Activated by Tumor Acidity for Orchestrated Oxidation/Chemotherapy. *Nano Lett.* **2017**, *17* (11), 6983−6990.
(62) Su, L.; Khan, S.; Fan, J.; Lin, Y.-N.; Wang, H.; Gustafson, T. P.; Zhang, F.; Wooley, K. L. Functional sugar-based polymers and nanostructures comprised of degradable poly(D-glucose carbonate)s. *Polym. Chem.* **2017**, *8* (10), 1699−1707.
(63) Lin, Y.-N.; Su, L.; Smolen, J.; Li, R.; Song, Y.; Wang, H.; Dong, M.; Wooley, K. L. Co-assembly of sugar-based amphiphilic block polymers to achieve nanoparticles with tunable morphology, size, surface charge, and acid-responsive behavior. *Mater. Chem. Front.* **2018**, *2* (12), 2230−2238.
(64) Osumi, S.; Felder, S. E.; Wang, H.; Lin, Y.-N.; Dong, M.; Wooley, K. L. Construction of nanostructures in aqueous solution from amphiphilic glucose-derived polycarbonates. *J. Polym. Sci., Part A: Polym. Chem.* **2019**, *57* (3), 432−440.
(65) Dong, M.; Song, Y.; Wang, H.; Su, L.; Shen, Y.; Tran, D. K.; Letteri, R. A.; Flores, J. A.; Lin, Y.-N.; Li, J.; Wooley, K. L., Degradable sugar-based magnetic hybrid nanoparticles for recovery of crude oil from aqueous environments. *Polym. Chem.* **2020**, in press. DOI: 10.1039/D0PY00029A
(66) Schaefer, T.; Reynolds, W. F.; Yonemoto, T. Possible Intramolecular Van der Waals Contributions to Proton and Carbon-13 Shifts in Aliphatic and Aromatic Halogen Compounds. *Can. J. Chem.* **1963**, *41* (12), 2969−2976.
(67) Gil, V. M. S.; Gibbons, W. A. Effect of intramolecular Van der Waals forces on N.M.R. spectra. *Mol. Phys.* **1964**, *8* (2), 199−200.
(68) Li, S.; Chesnut, D. B. Intramolecular van der waals interactions and chemical shifts: A model for β- and γ-effects. *Magn. Reson. Chem.* **1985**, *23* (8), 625−638.
(69) Zhang, F.; Ni, Q.; Jacobson, O.; Cheng, S.; Liao, A.; Wang, Z.; He, Z.; Yu, G.; Song, J.; Ma, Y.; Niu, G.; Zhang, L.; Zhu, G.; Chen, X. Polymeric Nanoparticles with a Glutathione-Sensitive Heterodimeric Multifunctional Prodrug for *In Vivo* Drug Monitoring and Synergistic Cancer Therapy. *Angew. Chem., Int. Ed.* **2018**, *57* (24), 7066−7070.
(70) Heintz, A.; Odicino, F.; Maisonneuve, P.; Quinn, M.; Benedet, J.; Creasman, W.; Ngan, H.; Pecorelli, S.; Beller, U. Carcinoma of the Ovary. *Int. J. Gynecol. Obstet.* **2006**, *95* (S1), S161−S192.
(71) Venditto, V. J.; Simanek, E. E. Cancer Therapies Utilizing the Camptothecins: A Review of the *In Vivo* Literature. *Mol. Pharmaceutics* **2010**, *7* (2), 307−349.
(72) Gershenson, D. M. Irinotecan in epithelial ovarian cancer. *Oncology (Williston Park)* **2002**, *16* (5), 29−31.
(73) Bodurka, D. C.; Levenback, C.; Wolf, J. K.; Gano, J.; Wharton, J. T.; Kavanagh, J. J.; Gershenson, D. M. Phase II Trial of Irinotecan in Patients With Metastatic Epithelial Ovarian Cancer or Peritoneal Cancer. *J. Clin. Oncol.* **2003**, *21* (2), 291−297.
(74) Musa, F.; Pothuri, B.; Blank, S. V.; Ling, H. T.; Speyer, J. L.; Curtin, J.; Boyd, L.; Li, X.; Goldberg, J. D.; Muggia, F.; Tiersten, A. Phase II study of irinotecan in combination with bevacizumab in recurrent ovarian cancer. *Gynecol. Oncol.* **2017**, *144* (2), 279−284.
(75) Wang, Y.; Probin, V.; Zhou, D. Cancer therapy-induced residual bone marrow injury-Mechanisms of induction and implication for therapy. *Curr. Cancer Ther. Rev.* **2006**, *2* (3), 271−279.
(76) Shao, L.; Wang, Y.; Chang, J.; Luo, Y.; Meng, A.; Zhou, D. Hematopoietic stem cell senescence and cancer therapy-induced long-term bone marrow injury. *Transl. Cancer Res.* **2013**, *2* (5), 397−411.
(77) Verma, R.; Foster, R. E.; Horgan, K.; Mounsey, K.; Nixon, H.; Smalle, N.; Hughes, T. A.; Carter, C. R. D. Lymphocyte depletion and repopulation after chemotherapy for primary breast cancer. *Breast Cancer Res.* **2016**, *18* (1), 10.
(78) Calvi, L. M.; Adams, G. B.; Weibrecht, K. W.; Weber, J. M.; Olson, D. P.; Knight, M. C.; Martin, R. P.; Schipani, E.; Divieti, P.; Bringhurst, F. R.; Milner, L. A.; Kronenberg, H. M.; Scadden, D. T. Osteoblastic cells regulate the haematopoietic stem cell niche. *Nature* **2003**, *425* (6960), 841−846.

https://dx.doi.org/10.1021/acs.nanolett.0c02319
Nano Lett. 2020, 20, 6563−6571